Geophysical Research Letters

RESEARCH LETTER
10.1029/2019GL084351

Key Points:
- Only after NH_x reduction exceeds 25% can ammonia control effectively reduce the inorganic aerosol mass
- More NHx reduction will be required to reach the critical point of effective ammonia control as NO_x and SO_2 emissions decrease
- A large enough NH_x reduction (60%–80%) renders concurrent reduction of NO_x emissions ineffective and even the effect of SO_2 emission control is reduced

Supporting Information:
- Supporting Information S1

Correspondence to:
Y. Wang, and S. Kong,
yuhang.wang@eas.gatech.edu;
kongshaofei@cug.edu.cn

Citation:
Zheng, M., Wang, Y., Bao, J., Yuan, L., Zheng, H., Yan, Y., et al. (2019). Initial cost barrier of ammonia control in central China. *Geophysical Research Letters*, *46*. https://doi.org/10.1029/2019GL084351

Received 30 JUN 2019
Accepted 5 NOV 2019
Accepted article online 11 NOV 2019

Initial Cost Barrier of Ammonia Control in Central China

Mingming Zheng[1,2,3], Yuhang Wang[2], Jianguo Bao[1], Lianxin Yuan[3], Huang Zheng[1], Yingying Yan[1], Dantong Liu[4], Mingjie Xie[5], and Shaofei Kong[1]

[1]School of Environmental Studies, China University of Geosciences, Wuhan, China, [2]School of Earth and Atmospheric Sciences, Georgia Institute of Technology, Atlanta, GA, USA, [3]Hubei Environment Monitoring Center, Wuhan, China, [4]School of Earth Sciences, Zhejiang University, Zhejiang, China, [5]Collaborative Innovation Center of Atmospheric Environment and Equipment Technology, Jiangsu Key Laboratory of Atmospheric Environment Monitoring and Pollution Control, School of Environmental Science and Engineering, Nanjing University of Information Science and Technology, Nanjing, China

Abstract Ammonia control has received increasing attention as a measure to decrease particulate concentrations. Modeling analysis of observation data from central China over the period of September 2015 to August 2016 shows clear asymmetric responses of particulate pH and mass to ammonia emissions. With a change of ±80% of NH_x ($NH_3 + NH_4^+$), the corresponding ΔpH are +0.5 and −3.0, respectively, and the corresponding particulate NH_4^+ changes are +2.62% and −61.8%, respectively. This asymmetry implies that there is a Critical Total Ammonia Concentration, above which particulate pH and mass are insensitive to ammonia control. Analysis of the observation data suggests that the Critical Total Ammonia Concentration is −25%. The estimated cost for an NH_x reduction of 25% is \$140 – 320 million for Hubei province, which is the initial cost barrier before ammonia control can effectively affect particulate pH and mass in central China. This cost barrier will increase as NO_x and SO_2 emissions decrease.

1. Introduction

Aerosol acidity is one factor that impacts organic (Cao & Jang, 2010; Jang et al., 2002; Pathak et al., 2011; Surratt et al., 2007) and inorganic secondary aerosol formation (Manktelow et al., 2010; Underwood et al., 2001; Wang et al., 2016) through gas-particulate phase partitioning (Grassian, 2001; Keene et al., 2004), acid-catalyzed heterogeneous reactions (Jang et al., 2002; Nemitz et al., 2004; Xu et al., 2015), and the migration of redox minerals and metals (Meskhidze et al., 2003). It is also an area of concern considering its environmental effects (Liu et al., 2017; Tian et al., 2018; Zhou et al., 2018).

As the primary alkaline gas in atmosphere (Seinfeld & Pandis, 2006; Sun & Wexler, 1998; Wang et al., 2015), ammonia (NH_3) is mainly emitted from agricultural activities, including fertilizer application, livestock waste volatilization, and crop burning (Huang et al., 2012; Reis et al., 2009; Van Damme et al., 2014; Zhang et al., 2017). Industrial and vehicle emissions are also important sources in urban areas (Livingston et al., 2009; Suarez-Bertoa et al., 2014). Ammonia emission control has received a lot of attention especially for controlling the severe haze pollution in China. Wang et al. (2011) speculated that a 90% increase in ammonia emissions during 1990 – 2005 contributed to about a 50% – 60% increase in sulfate and nitrate aerosol concentrations. NO_3^- will be further enhanced if ammonia emissions are not reduced, and the reduction in ammonia emissions is beneficial to $PM_{2.5}$ control for most regions (Wang et al., 2011). Recently, An et al. (2019) indicated a 50% reduction in ammonia yielded a 10% reduction in $PM_{2.5}$ in a haze event in North China. Liu et al. (2019) also implied that a 50% reduction in ammonia emissions with a 15% reduction in sulfur dioxide and nitrogen oxides can reduce $PM_{2.5}$ by 11% − 17%. On the other hand, Guo et al. (2018) suggested that the effect of NH_x control on reducing ionic masses of $PM_{2.5}$ is not as good as controlling TNO_3 and SO_4^{2-} unless NH_x is reduced by more than 60% in Beijing.

Particulate mass control by ammonia emission reduction is affected by particulate pH (Guo et al., 2018). However, particulate pH is determined by many factors, such as chemical components and meteorological conditions (He et al., 2012; Liu et al., 2017). Few studies investigated particulate pH variation with changes (both increases and decreases) in chemical and meteorological parameters. Ammonia is a key factor affecting aerosol acidity due to its alkaline property (Liu et al., 2017) although the effect of ammonia on aerosol pH is buffered (Weber et al., 2016).

Based on 1-year continuous observation of hourly water-soluble inorganic ions in $PM_{2.5}$ and precursor gases from September 2015 to August 2016, the sensitivities of chemical components and meteorological parameters using a thermodynamic model were carried out to assess the influence of each component on particulate pH and aerosol water content (AWC). Specifically, the responses of pH and fine particle mass to different ammonia emission change scenarios and the significance of increasing or decreasing ammonia emissions for particulate mass control were investigated. By exploring the observation-based sensitivities, we defined a Critical Total Ammonia Concentration (CTAC), which is the inflection point of effective ammonia control for particulate mass reduction. Hence, there is an initial cost barrier of ammonia control, significant impacts of which are realized only after the economic expense of ammonia emission reduction to reach the CTAC.

2. Method and Model

2.1. Observation

The observation site (30.53°E, 114.36°N) is located at a representative residential/commercial mixed area with no nearby industrial emissions in Wuhan city, central China (Figure S1 and Text S1 in the supporting information). Water-soluble ions including SO_4^{2-}, NO_3^-, NH_4^+, Cl^-, K^+, Na^+, Mg^{2+}, and Ca^{2+} in $PM_{2.5}$ and gaseous HNO_3, HCl, and NH_3 were synchronously monitored by an online ion chromatography analyzer (MARGA-ADI 2080) with 1-hour resolution (Li et al., 2019). A wet rotating denuder was used to collect the gases. Aerosols were collected by a steam jet aerosol collector with a $PM_{2.5}$ cyclone inlet. Gas and aerosol liquid extracts were analyzed by ion chromatograph. The sampling flow rate for the MARGA system was 16.7 L min^{-1}. Details about its maintenance can be found in previous literature (Rumsey et al., 2014). Quality assurance and quality control for the MARGA system were also performed (Text S2). Continuous hourly monitoring was carried out over 1 year, from September 2015 to August 2016, with no data collected in February due to equipment maintenance. Data for periods of precipitation and dust storms were excluded. Hourly $PM_{2.5}$, NO_2, and SO_2 were measured by β-ray, chemiluminescence, and ultraviolet fluorescence online monitoring equipment, respectively. Meteorological parameters including temperature and RH were obtained from a local observatory. The data quality check can be found in Text S3.

2.2. pH Calculation

The thermodynamic model ISOROPPIA-II (http://nenes.eas.gatech.edu/ISORROPIA) (Fountoukis & Nenes, 2007; Nenes et al., 1998) was applied to compute particulate pH, AWC, and the partition between gas and particulate phases. Model inputs include observed SO_4^{2-}, NH_4^+, NO_3^-, Cl^-, Na^+, K^+, Mg^{2+}, Ca^{2+}, ambient RH, T, and gaseous precursors (NH_3, HNO_3, and HCl) (Murphy et al., 2017; Song et al., 2018). The forward mode with metastable state was employed due to its better performance (Fountoukis & Nenes, 2007; Guo et al., 2015; Guo et al., 2016; Hennigan et al., 2015; Weber et al., 2016). The observed RH in this study are all above 20% which fits the model assumption of inorganic ions being in aqueous phase (Ansari & Pandis, 2000; Malm & Day, 2001; Fountoukis & Nenes, 2007; Bertram et al., 2011; Guo et al., 2017;). The calculated inorganic partitioning by ISOROPPIA-II agreed well with their measured concentrations (Figure S3).

3. Results

3.1. Responses of Particulate pH and AWC to Chemical and Meteorological Parameters

The $PM_{2.5}$ mass concentration in Wuhan averaged 65.3 ± 41.5 μg m^{-3} annually (Table S3), approximately 1.9 times the annual secondary ambient air quality standard of $PM_{2.5}$ in China. Sulfate, nitrate, and ammonium were the dominant components, accounting for 23.7%, 22.3%, and 16.1% of $PM_{2.5}$, respectively. The aerosol pH in Wuhan varied in the range of 1.54 – 4.65, with a mean value of 3.27, suggesting moderate aerosol acidity (Figure S4). It was higher in winter (3.69) than summer (2.86); the seasonal difference was in agreement with previous studies (Table S4). The monthly variation of pH was similar to that of AWC (Figure S4) as was found by Liu et al. (2017).

To further explore the impacts of chemical and meteorological parameters on particulate pH and AWC, changes in pH and AWC (ΔpH and ΔAWC) were evaluated corresponding to the changes of SO_4^{2-}, TNO_3 (NO_3^- + HNO_3), NH_x (NH_3 + NH_4^+), TCl (Cl^- + HCl), RH and T, respectively. Each component was

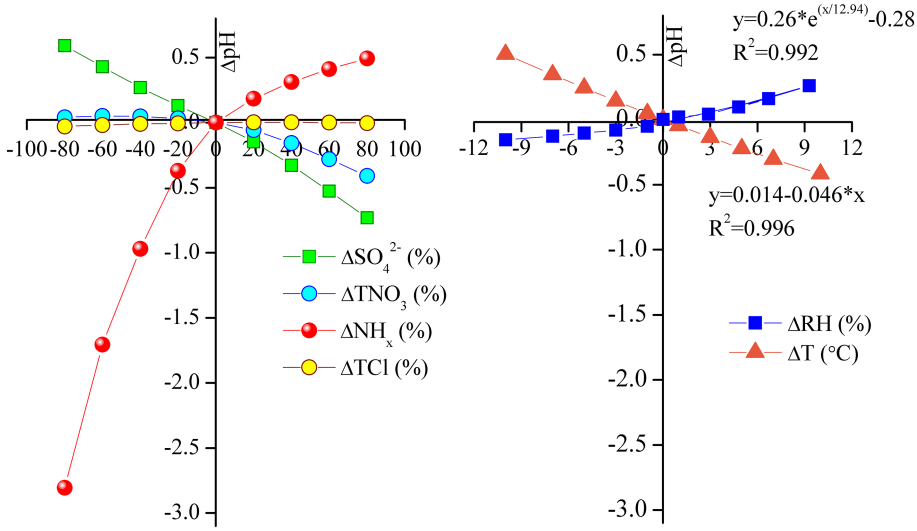

Figure 1. Sensitivity analysis of ΔpH (pH changes) to the change in SO_4^{2-}, TNO_3 (NO_3^- + HNO_3), NH_x (NH_3 + NH_4^+), TCl (Cl^- + HCl), RH, and T, respectively. Each pollutant is increased or decreased in steps from 0% to 80%, while keeping the other model inputs constant. The ranges for RH and T changes are ±10% and ±10 °C, respectively.

increased or decreased in steps from 0% to 80%, while the other model inputs were kept constant. For the sensitivities of meteorological parameters, the values of RH and T were changed in a range of ±10% and ±10 °C, respectively, while the other inputs were kept constant. The range of RH sensitivity was regulated between the upper limit of 100% and the lower limit of 20% along with the actual RH variation in Wuhan. Corresponding responses of pH were shown in Figure 1. The base value corresponded to 0% expansion and reduction in all plots.

Figure 1 shows the sensitivity results. The pH values responded linearly to SO_4^{2-} variation since SO_4^{2-} is nonvolatile. The range of ΔpH was −0.73 – 0.59 when SO_4^{2-} varied by ±80%. A least squares regression gave a slope of $\partial pH/\partial SO_4^{2-} \approx -0.007$ ($m^3\ \mu g^{-1}$) ($R^2 = 0.61$), implying that pH increased (decreased) 0.14 unit with SO_4^{2-} decreasing (increasing) by 20%. In the case of TNO_3 change, particulate pH only changed slightly when TNO_3 increased, with a 0.41 unit decrease in pH when TNO_3 increased by 80%. For Wuhan, a decrease of TNO_3 did not obviously affect particulate pH. The sensitivity of particulate pH to TCl is also very low.

In comparison to SO_4^{2-}, TNO_3, and TCl, the effect of NH_x can be much larger. While the increase of pH with increasing NH_x was moderate, the decrease of pH with decreasing NH_x was logarithmic. Corresponding to an 80% change of NH_x, the increase of pH was 0.5 unit but the decrease of pH (due to NH_x reduction) was about 3.0 units, that is, that particulate [H^+] increased by 3 orders of magnitudes. This large asymmetric response of particulate pH to NH_x was due to the changes of AWC and semivolatile NH_x partitioning (Bougiatioti et al., 2016; Guo et al., 2016; Weber et al., 2016), which we will discuss further in section 3.2.

A partial derivative $\partial pH/\partial T \approx -0.05$ ($°C^{-1}$) was obtained for pH dependence on temperature, suggesting a 0.1-unit decrease (increase) of particulate pH with a temperature increase (decrease) by 2 °C. An exponential relationship between ΔpH and ΔRH was found. Considering the objectivity and insignificant interannual fluctuations of RH and T, as reported −0.81%/10 years of RH (Suonan et al., 2018) in Wuhan, more attention should be paid to the influence of anthropogenic and controllable pollutants changes on aerosol acidity, especially that of NH_x.

The effects of SO_4^{2-}, TNO_3, NH_x, TCl, RH, and T changes on AWC were shown in Figure 2. AWC showed nearly linear variations with ΔTNO_3, ΔSO_4^{2-}, and ΔTCl. ΔTNO_3 exhibited a more obvious impact on ΔAWC than ΔSO_4^{2-} and ΔTCl in part because NO_3^- molar concentrations were higher than SO_4^{2-} and Cl^- (Table S3). In the range of particulate pH in Wuhan, nearly all TNO_3 was in the particulate phase (Figure S5).

As pH, the largest AWC sensitivity was found for NH_x and the sensitivity was highly asymmetric. While there was a negligible increase of AWC with ΔNH_x increasing from 0% to 80%, AWC decreased by nearly

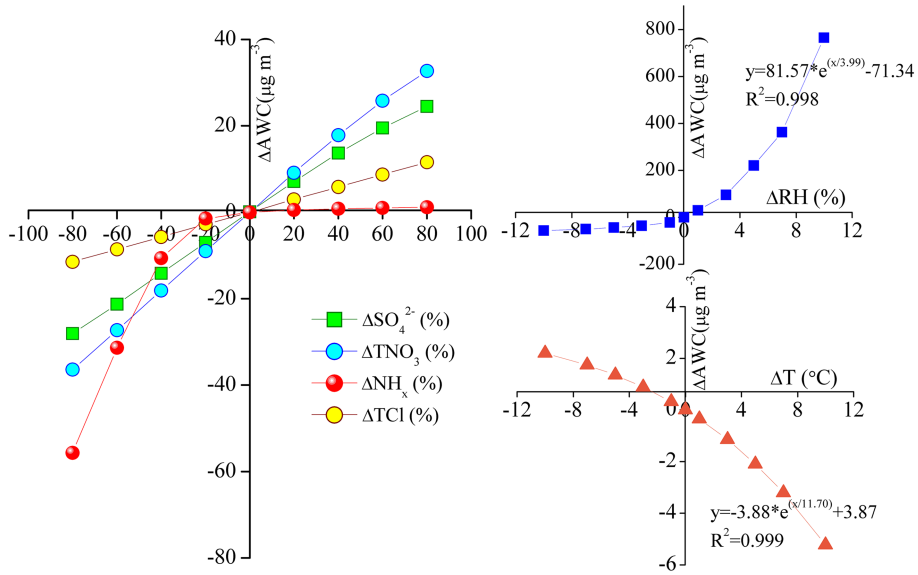

Figure 2. Same as Figure 1 but for ΔAWC.

60% with a NH_x decrease of 80%. The asymmetric response was due in part to the gas-particulate partition of NH_x as a function of pH (Figure S5). The increase of NH_x only increased NH_3 concentrations in the gas phase but not particulate NH_4^+, leading to no changes in AWC. As NH_x decreased, particulate pH decreased (Figure 1) and the particulate NH_4^+ fraction in NH_x, ε (NH_4^+), increased toward 100%. Besides, and the particulate NO_3^- fraction, ε (NO_3^-), decreased toward zero as to pH decreases when NH_x descent (Figure S5). As a result, the reduction of NH_x led to a corresponding reduction of NH_4^+ and NO_3^- water uptake.

For meteorological parameters, Figure 2 shows that the change of T had a relatively weak impact on AWC, within only a 5 μg m^{-3} AWC change when ΔT varied by ±10 °C. However, AWC increased by almost an order of magnitude when RH increased by 10%, explaining a tendency towards hazy conditions when RH was high in Wuhan.

3.2. Asymmetric Responses of Inorganic Particulate Mass to NH_x Changes

We explored the asymmetric responses of total water-soluble ions (WSI, including SO_4^{2-}, NO_3^-, NH_4^+, Cl^-, HSO_4^-, K^+, Na^+, Mg^{2+}, and Ca^{2+}) to NH_x changes in Figure 3. In addition to WSI, [NH_4^+], [H^+], and ΔAWC, all showed little responses when NH_x increased but logarithmic or exponential changes when NH_x decreased. With an NH_x decrease of 80%, WSI, [NH_4^+], and ΔAWC decreased by 21.6, 6.2, and 55.6 μg m^{-3}, respectively. We added more calculations with a step change of 1% NH_x reduction in the range of −40% – 0% ΔNH_x to explore the transition from slow to fast responses of WSI and the other parameters. We defined the inflection point of the WSI response sensitivity as the CTAC. With the detailed calculations, we found that the CTAC, where the first-order derivative change from the left side to the right side was largest or the absolute second-order derivative of WSI to NH_x was at a maximum, for Wuhan is −25% ([NH_x] at 14.3 μg m^{-3}). When NH_x reduction exceeded this value, the changes of WSI and other parameters accelerated. The CTAC corresponded to a reduction of [NH_4^+] by 4.84%.

The physical meaning of the CTAC can also be understood by looking at the cumulative changes. From the CTAC (−25%) to an NH_x decrease of −80%, WSI decreased by 49%. In comparison, from the CTAC (−25%) to an NH_x increase of 80%, WSI increased only by 7%. The large asymmetric sensitivity on the left and right sides of the CTAC was largely due to increasing partitioning of NH_x to the particulate phase (Figures 3 and S5) but decreasing TNO_3 partitioning into the particulate phase (Figures 1 and S5), the logarithmic decrease of AWC (Figure 2), and the exponential increase of [H^+] (Figure 3), when NH_x decreased on the left side of the CTAC. AWC response to NH_x change has similar asymmetry as that of WSI due to corresponding changes of water uptake by NH_4^+ and NO_3^-.

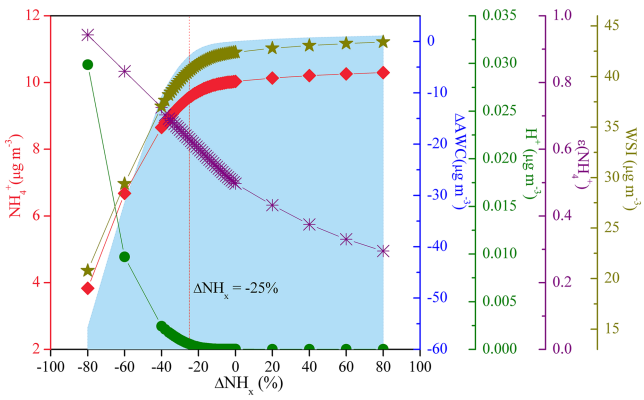

Figure 3. Changes of ΔAWC, [H^+], [NH_4^+], WSI, and ε (NH_4^+) as functions of ΔNH_x. The red dashed vertical line denotes the CTAC of −25%.

The WSI decrease was a factor of 3.4 larger than that of [NH_4^+] due to the increasing TNO_3 partitioning into gas phase and the corresponding loss of [NO_3^-] as pH decreased (Figure S5) when NH_x reduction decreased from the CTAC to −80%. The average particulate pH at the CTAC was 2.76, corresponding to an ε (NH_4^+) value of 0.63. When NH_x decreased from the CTAC to −80%, the average pH decreased from 2.76 to 0.47. Consequently, ε (NH_4^+) approached 100%, that is, the reduction of NH_x leads to an equivalent loss of [NH_4^+]. Furthermore, ε (NO_3^-) decreased from 97.7% to 17.9%, suggesting that the majority of particulate NO_3^- degassed, reducing WSI. In comparison, when NH_x increased from the CTAC to 80%, the average particulate pH increased from 2.76 to 3.76 and the corresponding ε (NO_3^-) and [NH_4^+] increases of 2.1% and 7.7%, respectively, were relatively small.

The −25% CTAC point is quite robust. If we only use the observation data in the 62 days when daily $PM_{2.5}$ is larger than the ambient air quality standard of China (75 μg m^{-3}), the CTAC value is still −25%. If we use the data in the 29 winter days of daily $PM_{2.5}$ > 75 μg m^{-3}, the CTAC value is −22%. Almost all high $PM_{2.5}$ winter days were in December and January because of instrument malfunction and maintenance in February.

3.3. Decrease of the CTAC With SO_4^{2-} or TNO_3 Reduction

The CTAC value depends on the concentrations of SO_4^{2-} and TNO_3. Given the continued efforts in China to reduce the emissions of sulfur dioxide and nitrogen oxide (Jin et al., 2016; Zheng et al., 2018), the CTAC values will likely change in the future. We conducted a suite of modeling scenarios in which SO_4^{2-} or TNO_3 was decreased by 20% or 50%. The CTAC values were at −31%, −32%, −39%, and −42% of ΔNH_x for reducing 20% of SO_4^{2-}, 20% of TNO_3, 50% of SO_4^{2-}, and 50% of TNO_3, respectively. As expected, these values were lower than −25%, reflecting a need to reduce NH_x further before the effect of ammonia control can be realized. The corresponding average pH values were 2.88, 2.73, 3.12, and 2.64, respectively. The average ε (NH_4^+) values were 0.60, 0.63, 0.54, and 0.62, and the average NH_x concentrations were 13.8, 13.6, 12.4, and 11.7 μg m^{-3}, respectively (Figure 4).

At a reduction of 50%, Figure 4 shows that TNO_3 reduction decreased the CTAC value more than SO_4^{2-} due in part to the semivolatile nature of NH_x and TNO_3. Given the average condition of the observation data, a 50% reduction of SO_4^{2-} led to a lager decrease of NH_4^+ than that of TNO_3 since ε (NH_4^+) was lower and pH was higher in the former (Figure 4). As NH_x reduction increased, the difference of pH between SO_4^{2-} and TNO_3 reductions became larger, which can be more clearly seen in the changes of [H^+]. As a result, more NH_x was partitioned into the particulate phase with TNO_3 reduction than that of SO_4^{2-} and a larger CTAC value was needed in the former.

At an NH_x reduction of 80%, Figure 4 shows that the concentrations of WSI were similar regardless of the scenarios of TNO_3 reductions. Most TNO_3 was shifted into gas phase due to low pH at large NH_x reductions (Seinfeld & Pandis, 2006; Guo et al., 2018; Figure S5). The effect of increasing TNO_3 gas-phase partition can be more clearly seen in Figure S6. We subtracted the WSI concentration in a scenario with 20% or 50% reduction of SO_4^{2-} or TNO_3 from the base scenario with no such reduction. For ΔNH_x > 0, the computed ΔWSI values between the reduction and base scenarios were similar for SO_4^{2-} or TNO_3 at the same reduction level. As NH_x reduction increased, the corresponding ΔWSI reduction decreased due mostly to the shifting partition of TNO_3 to gas phase. Large deviations were found for the effect of TNO_3 from SO_4^{2-} reduction scenarios at an NH_x reduction of 60% – 80%. At 60% NH_x reduction, ΔWSI of 50% TNO_3 reduction approached that of 20% SO_4^{2-} reduction. At 80% NH_x reduction, concurrent TNO_3 reduction had little effect on ΔWSI, while the effect of concurrent SO_4^{2-} reduction of 50% was half of the no SO_4^{2-} reduction scenario (Figures 4 and S6).

The differential effects of concurrent TNO_3 from SO_4^{2-} reduction at large NH_x reductions can be clearly seen in Figure S7. In the scenario of a current reduction of 20% or 50% TNO_3, the decreases of Δ[NH_4^+]

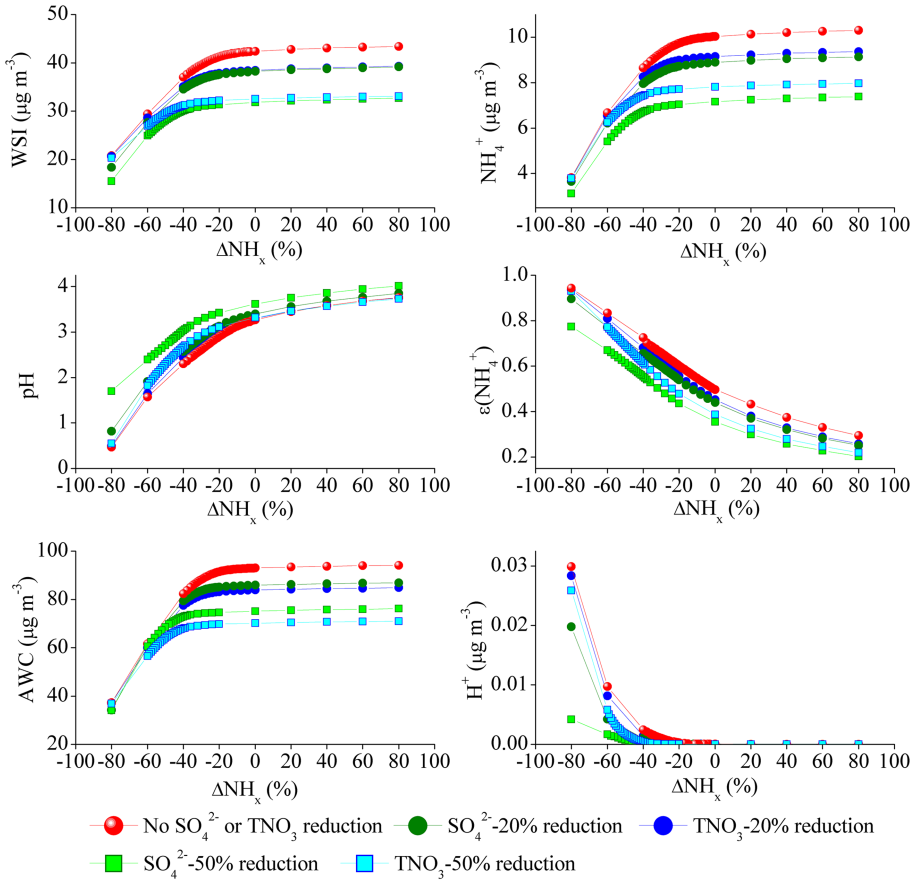

Figure 4. Changes of WSI, $[NH_4^+]$, particulate pH, ε (NH_4^+), AWC, and $[H^+]$ as functions of ΔNH_x for different scenarios: no SO_4^{2-} or TNO_3 reduction (red), 20% reduction of SO_4^{2-} (dark green), 20% reduction of TNO_3 (blue), 50% reduction of SO_4^{2-} (light green), and 50% reduction of TNO_3 (cyan).

and $\Delta[NO_3^-]$, relative to no TNO_3 reduction scenario, were monotonic with decreasing NH_x. However, in the scenario of a concurrent reduction of 20% or 50% SO_4^{2-}, $\Delta[NO_3^-]$ increased with decreasing NH_x. Figure S8 helps explain the differential effects. The major cations (NH_4^+, K^+, Ca^{2+}, Na^+, Mg^{2+}, and H^+) were in balance with major anions (SO_4^{2-}, NO_3^-, HSO_4^-, and Cl^-). The ratio of $[NO_3^-]$ to the sum of $[NH_4^+]$ and $[H^+]$ was much more sensitive to SO_4^{2-} than TNO_3 reduction because of the partitioning of TNO_3 between gas and particulate phases (Figures S8 and S9). At an NH_x reduction of 80%, $[H^+]$ increased to be in the same order of magnitude of $[NH_4^+]$ and therefore we used the sum of $[NH_4^+]$ and $[H^+]$ as the denominator in Figure S8. Higher SO_4^{2-} and lower NH_x tend to lead to more TNO_3 partitioning to gas phase. In the scenario of no SO_4^{2-} or TNO_3 reduction, decreasing NH_x led to increasing partitioning of TNO_3 to gas phase and smaller ΔWSI reductions due to concurrent TNO_3 reductions (Figures S6 and S7). At an 80% reduction of NH_x, the effect of concurrent TNO_3 reduction on ΔWSI was close to 0.

Contrary to the reduction of TNO_3, concurrent reduction of SO_4^{2-} by 20% or 50% increased the ratio of $[NO_3^-]/([NH_4^+] + [H^+])$ relative to the base scenario of no SO_4^{2-} or TNO_3 reduction and this increase was larger with increasing NH_x reduction (Figure S9). Figure S7 shows that $\Delta[NO_3^-]$ was positive with decreasing NH_x in the 20% or 50% SO_4^{2-} scenario in contrast to the TNO_3 reduction scenarios. Compared to the scenario of no SO_4^{2-} or TNO_3 reduction, the effect of concurrent SO_4^{2-} reduction on ΔWSI decreased with decreasing NH_x (Figure S6) because of the decrease of $\Delta[NH_4^+]$ reduction and increase of $\Delta[NO_3^-]$ (Figure S7). When NH_x reduction increased from 60% to 80%, $\Delta[NH_4^+]$ reduction continued decreasing but $\Delta[NO_3^-]$ also decreased, leading to a small increase of ΔWSI reduction (Figure S6). In the scenario of no SO_4^{2-} or TNO_3 reduction, the decrease of the molar ratio of $[NO_3^-]/([NH_4^+] + [H^+])$ from a reduction

of NH_x from 60% to 80% was similar to the 50% SO_4^{2-} reduction scenario (Figure S8); the difference of $[NH_4^+] + [H^+]$ between the two scenarios was smaller at an 80% NH_x reduction (Figure S10), leading to a smaller $\Delta[NO_3^-]$ between the two scenarios at the 80% than 60% reduction of NH_x (Figure S7). Furthermore, in the scenario of no SO_4^{2-} reduction, the ratio of $[NO_3^-]/([NH_4^+] + [H^+])$ approached 9.9% (Figure S8), meaning that most of TNO_3 was in gas phase and it was difficult to decrease ΔWSI reduction through partitioning TNO_3 into gas phase. Further NH_x reduction would lead to increases of $[H^+]$ and $[HSO_4^-]$ instead. In contrast, with a concurrent 50% reduction of SO_4^{2-}, the ratio of $[NO_3^-]/([NH_4^+] + [H^+])$ stayed at 40% with an 80% NH_x reduction, leaving a large room to further partition TNO_3 into gas phase.

The CTAC is a quantitative threshold value for the effectiveness of ammonia control on aerosol WSI mass. Previous studies noted that this effectiveness depends on aerosol thermodynamic equilibrium between NH_x and the sum of TNO_3 and the net negative charge excluding NH_4^+ and H^+; Blanchard et al. (2000) defined the difference between the two terms as excess NH_3, and Xu et al. (2019) defined the molar ratio of the two terms as R. The theoretical indicators for the transition of NH_x partition are 0 and 1 for excessive NH_3 and R, respectively (Blanchard et al., 2000; Xu et al., 2019). Furthermore, Guo et al. (2018) suggested that effective NH_3 reduction occurs at pH < 3. In this study, we find that the CTAC values (including the observation data and 20% and 50% reductions of SO_4^{2-} or TNO_3) correspond to excess NH_3 of 0.18 – 0.24 μmol m^{-3}, R values of 1.39 – 1.53, and pH values of 2.64 – 3.12, reflecting the complexity in aerosol thermodynamics. Our results indicate that the CTAC point is reached with NH_x molar concentrations 39% – 53% higher than the theoretical threshold of $R = 1$ when NH_x molar concentration equals to the sum of TNO_3 and the net negative charge excluding NH_4^+ and H^+.

4. Initial Cost Barrier

In controlling particular mass via ammonia reduction, the CTAC of −25% represents an initial economic cost barrier before the control measure becomes effective. Here we applied this CTAC value for the entire Hubei province. Wuhan is provincial capital and the largest city in the province and therefore emissions of SO_2 and NO_x are higher than other regions (Hong et al., 2018; Hubei Statistical Yearbook, 2018). On the other hand, over 90% of ammonia emissions in China are from agriculture, mainly fertilizer applications and livestock production (Huang et al., 2012; Reis et al., 2009; Van Damme et al., 2014; Zhang et al., 2017). Therefore, emissions of ammonia in Wuhan are comparable to other regions of the province. Analysis in the previous section showed that the CTAC values for rural Hubei would be < −25% with lower emissions of SO_2 and NO_x, and we used −25% as the lower cost estimate bound.

The total ammonia emission was estimated at 323.7 Gg (323,700 ton) for Hubei Province by Huang et al. (2012). Recently, Zhang et al. (2017) suggested a higher ammonia emission rates in central China at 30 – 50 kg N ha^{-1} in Hubei Province. Using the medium value of 40 kg N ha^{-1} for an area of 185,900 km^2 of Hubei province, the total ammonia emission is up to 743,600 tons. Among the various measures, controlling ammonia emissions in fertilizer applications is most cost effective (Liu et al., 2019; Pinder et al., 2007). Since fertilizer applications account for the largest portion of total ammonia emissions at 42.4% in Hubei province (Huang et al., 2012), we computed the initial cost barrier of ammonia control assuming that it all coming from improving fertilizer applications. As in Liu et al. (2019), we used an estimate of $1,700 per ton of ammonia emission reduction through improving fertilizer applications based on the work by Klimont and Winiwarter (2011) and obtained a total of $140–320 million for Hubei Province. In comparison, Liu et al. (2019) estimated a cost of $6.6 billion for a 50% ammonia emission reduction in China.

5. Conclusions

Using hourly water-soluble inorganic ions monitoring data collected from September 2015 to August 2016 in a megacity in central China, we analyzed the sensitivities of particulate pH and mass to NH_x changes. The average pH during the analysis period is 3.27 ± 0.49. Particulate pH and mass respond asymmetrically to NH_x change. This asymmetry is much stronger than the sensitivities of particulate pH and mass to SO_4^{2-} and TNO_3 changes. For example, increasing NH_x by 80% leads to a slight increase in pH by 0.5 and a 2.62% increase in NH_4^+. In contrast, an 80% decrease in NH_x results in a decrease of 3 and 61.8% in pH and NH_4^+, respectively.

Using model simulations, we compute the CTAC, above which particulate pH and mass are insensitive to ammonia reduction. The analysis of the observation data suggests that the CTAC is −25%. If we only use the data with daily $PM_{2.5} > 75$ μg m^{-3} in winter or all seasons, the results are similar. To reach this critical point of NH_x reduction, we estimate that the control cost for Hubei province is \$140 – 320 million; this is the initial cost barrier before ammonia control can effectively affect particulate pH and mass. A further issue is that the CTAC barrier increases as the emissions of SO_2 and NO_x decrease. Corresponding to a reduction of 20% in SO_4^{2-} or TNO_3, the CTAC value is −31% or −32%, respectively. If SO_4^{2-} or TNO_3 reduction is 50%, the CTAC is −39% or −42%, respectively. Consequently, the initial cost barrier for NH_x reduction will increase with the ongoing efforts on emission reductions in central China.

The CTAC is a quantitative threshold value for the effectiveness of ammonia control on aerosol WSI mass. In this study, we find that the CTAC values in the range of −25% to −42% (including the observation data and 20% or 50% reductions of SO_4^{2-} or TNO_3) correspond to excess NH_3 (Blanchard et al., 2000) of 0.18 – 0.24 μmol m^{-3}, molar ratio R values (Xu et al., 2019) of 1.39 – 1.53, pH values of 2.64 – 3.12, and ε (NH_4^+) values of 0.54 – 0.63. Significantly, the CTAC point (at R of 1.39 – 1.53) is reached much earlier than the theoretical threshold value of $R = 1$ for effective ammonia control. Despite this, we find a relatively large initial cost barrier based on the analysis of in situ observations, implying that the effectiveness of ammonia reduction (e.g., Liu et al., 2019) is low before reaching the CTAC point.

When a large enough NH_x reduction (60% – 80%) can be achieved, our analysis result indicates that the resulting WSI concentration decrease due to concurrent reduction of NO_x or SO_2 emissions is much reduced as the partitioning of TNO_3 shifted to gas phase. At an NH_x reduction of 80%, concurrent reduction of TNO_3 up to 50% has little effect on ΔWSI concentrations, while the effect of concurrent SO_4^{2-} reduction of 50% is half of no concurrent SO_4^{2-} reduction. Although the initial cost barrier of NH_x reduction is significant, after passing the CTAC, a large enough NH_x reduction can render the costs of TNO_3 and even some SO_4^{2-} reductions unnecessary to achieve a specific WSI reduction goal. However, large NH_x reductions beyond the CTAC will effectively decrease particulate mass but increase particulate acidity, the latter of which has negative consequences on the environment (e.g., Guo et al., 2018; Liu et al., 2019).

Acknowledgments
This study was financially supported by the Key Program of Ministry of Science and Technology of the People's Republic of China (2016YFA0602002 and 2017YFC0212602), the National Natural Science Fund (41830965), and the Key Program for Technical Innovation of Hubei Province (2017ACA089). Y. W. was supported by the National Science Foundation. Funding was also provided by the Start-up Foundation for Advanced Talents (162301182756) and the Fundamental Research Funds for the Central Universities (201616 and 201802), China University of Geosciences, Wuhan. We thank the two anonymous reviewers for their comments and suggestions. All data shown in the figures are included in the supporting information and are available at https://doi.org/10.6084/m9.figshare.10263080.

References

An, Z., Huang, R.-J., Zhang, R., Tie, X., Li, G., Cao, J., et al. (2019). Severe haze in northern China: A synergy of anthropogenic emissions and atmospheric processes. *Proceedings of the National Academy of Sciences of the United States of America*, *116*(18), 8657–8666. https://doi.org/10.1073/pnas.1900125116

Ansari, A. S., & Pandis, S. N. (2000). The effect of metastable equilibrium states on the partitioning of nitrate between the gas and aerosol phases. *Atmospheric Environment*, *34*(1), 157–168. https://doi.org/10.1016/S1352-2310(99)00242-3

Bertram, A. K., Martin, S. T., Hanna, S. J., Smith, M. L., Bodsworth, A., Chen, Q., et al. (2011). Predicting the relative humidities of liquid-liquid phase separation, efflorescence, and deliquescence of mixed particles of ammonium sulfate, organic material, and water using the organic-to-sulfate mass ratio of the particle and the oxygen-to-carbon elemental ratio of the organic component. *Atmospheric Chemistry and Physics*, *11*(21), 10,995–11,006. https://doi.org/10.5194/acp-11-10995-2011

Blanchard, C., Rose, P., Tanenbaum, S., Ziman, S., & Seinfeld, J. (2000). The use of ambient measurements to identify which precursor species limit aerosol nitrate formation. *J. Air Waste Manage*, *50*(12), 2073–2084. https://doi.org/10.1080/10473289.2000.10464239

Bougiatioti, A., Nikolaou, P., Stavroulas, I., Kouvarakis, G., Weber, R., Nenes, A., et al. (2016). Particle water and pH in the eastern Mediterranean: Source variability and implications for nutrient availability. *Atmospheric Chemistry and Physics*, *16*(7), 4579–4591. https://doi.org/10.5194/acp-16-4579-2016

Cao, G., & Jang, M. (2010). An SOA model for toluene oxidation in the presence of inorganic aerosols. *Environmental Science & Technology*, *44*(2), 727–733. https://doi.org/10.1021/es901682r

Fountoukis, C., & Nenes, A. (2007). ISORROPIA II: A computationally efficient thermodynamic equilibrium model for K^+-Ca^{2+}-Mg^{2+}-NH_4^+-Na^+-SO_4^{2-}-NO_3^--Cl^--H_2O aerosols. *Atmospheric Chemistry and Physics*, *7*(17), 4639–4659. https://doi.org/10.5194/acp-7-4639-2007

Grassian, V. H. (2001). Heterogeneous uptake and reaction of nitrogen oxides and volatile organic compounds on the surface of atmospheric particles including oxides, carbonates, soot and mineral dust: Implications for the chemical balance of the troposphere. *International Reviews in Physical Chemistry*, *20*(3), 467–548. https://doi.org/10.1080/01442350110051968

Guo, H., Liu, J., Froyd, K. D., Roberts, J. M., Veres, P. R., Hayes, P. L., et al. (2017). Fine particle pH and gas-particle phase partitioning of inorganic species in Pasadena, California, during the 2010 CalNex campaign. *Atmospheric Chemistry and Physics*, *17*(9), 5703–5719. https://doi.org/10.5194/acp-17-5703-2017

Guo, H., Otjes, R., Schlag, P., Kiendler-Scharr, A., Nenes, A., & Weber, R. J. (2018). Effectiveness of ammonia reduction on control of fine particle nitrate. *Atmospheric Chemistry and Physics*, *18*(16), 12,241–12,256. https://doi.org/10.5194/acp-18-12241-2018

Guo, H., Sullivan, A. P., Campuzano-Jost, P., Schroder, J. C., Lopez-Hilfiker, F. D., Dibb, J. E., et al. (2016). Fine particle pH and the partitioning of nitric acid during winter in the northeastern United States. *Journal of Geophysical Research: Atmospheres*, *121*, 10,355–10,376. https://doi.org/10.1002/2016JD025311

Guo, H., Xu, L., Bougiatioti, A., Cerully, K. M., Capps, S. L., Hite, J. R., et al. (2015). Fine-particle water and pH in the southeastern United States. *Atmospheric Chemistry and Physics*, *15*(9), 5211–5228. https://doi.org/10.5194/acp-15-5211-2015

He, K., Zhao, Q., Ma, Y., Duan, F., Yang, F., Shi, Z., & Chen, G. (2012). Spatial and seasonal variability of $PM_{2.5}$ acidity at two Chinese megacities: Insights into the formation of secondary inorganic aerosols. *Atmospheric Chemistry and Physics*, *12*(3), 1377–1395. https://doi.org/10.5194/acp-12-1377-2012

Hennigan, C. J., Izumi, J., Sullivan, A. P., Weber, R. J., & Nenes, A. (2015). A critical evaluation of proxy methods used to estimate the acidity of atmospheric particles. *Atmospheric Chemistry and Physics*, *15*(5), 2775–2790. https://doi.org/10.5194/acp-15-2775-2015

Hong, Q., Liu, C., Chan, K. L., Hu, Q., Xie, Z., Liu, H., et al. (2018). Ship-based MAX-DOAS measurements of tropospheric NO_2, SO_2, and HCHO distribution along the Yangtze River. *Atmospheric Chemistry and Physics*, *18*(8), 5931–5951. https://doi.org/10.5194/acp-18-5931-2018

Huang, X., Song, Y., Li, M., Li, J., Huo, Q., Cai, X., et al. (2012). A high-resolution ammonia emission inventory in China. *Global Biogeochemical Cycles*, *26*(1), GB1030. https://doi.org/10.1029/2011GB004161

Hubei provincial bureau of statistics (2018). Hubei statistical yearbook. Retrieved from http://tjj.hubei.gov.cn/.

Jang, M., Czoschke, N. M., Lee, S., & Kamens, R. M. (2002). Heterogeneous atmospheric aerosol production by acid-catalyzed particle-phase reactions. *Science*, *298*(5594), 814–817. https://doi.org/10.1126/science.1075798

Jin, Y., Andersson, H., & Zhang, S. (2016). Air pollution control policies in China: A retrospective and prospects. *International Journal of Environmental Research and Public Health*, *13*(12). https://doi.org/10.3390/ijerph13121219

Keene, W. C., Pszenny, A. A. P., Maben, J. R., Stevenson, E., & Wall, A. (2004). Closure evaluation of size-resolved aerosol pH in the New England coastal atmosphere during summer. *Journal of Geophysical Research, [Atmospheres]*, *109*(D23), D23307. https://doi.org/10.1029/2004JD004801

Klimont, Z., & Winiwarter, W. (2011). *Integrated ammonia abatement-modelling of emission control potentials and costs in GAINS, IIASA interim report*. Laxenburg, Austria: International Institute for Applied Systems Analysis (IIASA).

Li, H., Wang, D., Cui, L., Gao, Y., Huo, J., Wang, X., et al. (2019). Characteristics of atmospheric $PM_{2.5}$ composition during the implementation of stringent pollution control measures in shanghai for the 2016 G20 summit. *Science of The Total Environment*, *648*, 1121–1129. https://doi.org/10.1016/j.scitotenv.2018.08.219

Liu, M., Huang, X., Song, Y., Tang, J., Cao, J., Zhang, X., et al. (2019). Ammonia emission control in China would mitigate haze pollution and nitrogen deposition, but worsen acid rain. *Proceedings of the National Academy of Sciences of the United States of America*, *116*(16), 7760–7765. https://doi.org/10.1073/pnas.1814880116

Liu, M., Song, Y., Zhou, T., Xu, Z., Yan, C., Zheng, M., et al. (2017). Fine particle pH during severe haze episodes in northern China. *Geophysical Research Letters*, *44*(10), 5213–5221. https://doi.org/10.1002/2017GL073210

Livingston, C., Rieger, P., & Winer, A. (2009). Ammonia emissions from a representative in-use fleet of light and medium-duty vehicles in the California South Coast Air Basin. *Atmospheric Environment*, *43*(21), 3326–3333. https://doi.org/10.1016/j.atmosenv.2009.04.009

Malm, W. C., & Day, D. E. (2001). Estimates of aerosol species scattering characteristics as a function of relative humidity. *Atmospheric Environment*, *35*(16), 2845–2860. https://doi.org/10.1016/S1352-2310(01)00077-2

Manktelow, P. T., Carslaw, K. S., Mann, G. W., & Spracklen, D. V. (2010). The impact of dust on sulfate aerosol, CN and CCN during an East Asian dust storm. *Atmospheric Chemistry and Physics*, *10*(2), 365–382. https://doi.org/10.5194/acp-10-365-2010

Meskhidze, N., Chameides, W. L., Nenes, A., & Chen, G. (2003). Iron mobilization in mineral dust: Can anthropogenic SO_2 emissions affect ocean productivity? *Geophysical Research Letters*, *30* LO18035(21), 2085. https://doi.org/10.1029/2003GL018035

Murphy, J. G., Gregoire, P. K., Tevlin, A. G., Wentworth, G. R., Ellis, R. A., Markovic, M. Z., & VandenBoer, T. C. (2017). Observational constraints on particle acidity using measurements and modelling of particles and gases. *Faraday Discussions*, *200*(0), 379–395. https://doi.org/10.1039/C7FD00086C

Nemitz, E., Sutton, M. A., Wyers, G. P., & Jongejan, P. A. C. (2004). Gas-particle interactions above a Dutch heathland: I. Surface exchange fluxes of NH_3, SO_2, HNO_3 and HCl. *Atmospheric Chemistry and Physics*, *4*(4), 989–1005. https://doi.org/10.5194/acp-4-989-2004

Nenes, A., Pandis, S. N., & Pilinis, C. (1998). ISORROPIA: A new thermodynamic equilibrium model for multiphase multicomponent inorganic aerosols. *Aquatic Geochemistry*, *4*(1), 123–152. https://doi.org/10.1023/a:1009604003981

Pathak, R. K., Wang, T., Ho, K. F., & Lee, S. C. (2011). Characteristics of summertime $PM_{2.5}$ organic and elemental carbon in four major Chinese cities: Implications of high acidity for water-soluble organic carbon (WSOC). *Atmospheric Environment*, *45*(2), 318–325. https://doi.org/10.1016/j.atmosenv.2010.10.021

Pinder, R. W., Adams, P. J., & Pandis, S. N. (2007). Ammonia emission controls as a cost-effective strategy for reducing atmospheric particulate matter in the eastern United States. *Environmental Science & Technology*, *41*(2), 380–386. https://doi.org/10.1021/es060379a

Reis, S., Pinder, R. W., Zhang, M., Lijie, G., & Sutton, M. A. (2009). Reactive nitrogen in atmospheric emission inventories. *Atmospheric Chemistry and Physics*, *9*(19), 7657–7677. https://doi.org/10.5194/acp-9-7657-2009

Rumsey, I. C., Cowen, K. A., Walker, J. T., Kelly, T. J., Hanft, E. A., Mishoe, K., et al. (2014). An assessment of the performance of the Monitor for AeRosols and GAses in ambient air (MARGA): a semi-continuous method for soluble compounds. *Atmospheric Chemistry and Physics*, *14*(11), 5639–5658. https://doi.org/10.5194/acp-14-5639-2014

Seinfeld, J. H., & Pandis, S. N. (2006). *Atmospheric chemistry and physics: From air pollution to climate change* (Third ed.). Hoboken, NJ: John Wiley & Sons, Inc.

Song, S., Gao, M., Xu, W., Shao, J., Shi, G., Wang, S., et al. (2018). Fine-particle pH for Beijing winter haze as inferred from different thermodynamic equilibrium models. *Atmospheric Chemistry and Physics*, *18*(10), 7423–7438. https://doi.org/10.5194/acp-18-7423-2018

Suarez-Bertoa, R., Zardini, A. A., & Astorga, C. (2014). Ammonia exhaust emissions from spark ignition vehicles over the New European Driving Cycle. *Atmospheric Environment*, *97*, 43–53. https://doi.org/10.1016/j.atmosenv.2014.07.050

Sun, Q., & Wexler, A. S. (1998). Modeling urban and regional aerosols-condensation and evaporation near acid neutrality. *Atmospheric Environment*, *32*(20), 3527–3531. https://doi.org/10.1016/S1352-2310(98)00059-4

Suonan, K., Ren, G., Jia, W., & Sun, X. (2018). Climatological characteristics and long-term trend of relative humidity in Wuhan. *Climate and Environment Research (inChinese)*, *23*(6), 715–724. https://doi.org/10.3878/j.issn.1006-9585.2017.17122

Surratt, J. D., Lewandowski, M., Offenberg, J. H., Jaoui, M., Kleindienst, T. E., Edney, E. O., & Seinfeld, J. H. (2007). Evidence for organosulfates in secondary organic aerosol. *Environmental Science & Technology*, *41*, 517. https://doi.org/10.1021/es062081q

Tian, S., Pan, Y., & Wang, Y. (2018). Ion balance and acidity of size-segregated particles during haze episodes in urban Beijing. *Atmospheric Research*, *201*, 159–167. https://doi.org/10.1016/j.atmosres.2017.10.016

Underwood, G. M., Song, C. H., Phadnis, M., Carmichael, G. R., & Grassian, V. H. (2001). Heterogeneous reactions of NO_2 and HNO_3 on oxides and mineral dust: A combined laboratory and modeling study. *Journal of Geophysical Research*, *106*(D16), 18,055–18,066. https://doi.org/10.1029/2000JD900552

Van Damme, M., Clarisse, L., Heald, C. L., Hurtmans, D., Ngadi, Y., Clerbaux, C., et al. (2014). Global distributions, time series and error characterization of atmospheric ammonia (NH_3) from IASI satellite observations. *Atmospheric Chemistry and Physics*, *14*(6), 2905–2922. https://doi.org/10.5194/acp-14-2905-2014

Wang, G. H., Zhang, R. Y., Gomez, M. E., Yang, L. X., Levy Zamora, M., Hu, M., et al. (2016). Persistent sulfate formation from London Fog to Chinese haze. *P. Natl. Acad. Sci.*, *113*(48), 13,630–13,635. https://doi.org/10.1073/pnas.1616540113

Wang, S., Nan, J., Shi, C., Fu, Q., Gao, S., Wang, D., et al. (2015). Atmospheric ammonia and its impacts on regional air quality over the megacity of Shanghai, China. *Scientific Reports*, *5*, 15842. https://doi.org/10.1038/srep15842

Wang, S., Xing, J., Jang, C., Zhu, Y., Fu, J. S., & Hao, J. (2011). Impact assessment of ammonia emissions on inorganic aerosols in East China using response surface modeling technique. *Environmental Science & Technology*, *45*(21), 9293–9300. https://doi.org/10.1021/es2022347

Weber, R. J., Guo, H., Russell, A. G., & Nenes, A. (2016). High aerosol acidity despite declining atmospheric sulfate concentrations over the past 15 years. *Nature Geoscience*, *9*(4), 282–285. https://doi.org/10.1038/ngeo2665

Xu, L., Guo, H., Boyd, C. M., Klein, M., Bougiatioti, A., Cerully, K. M., et al. (2015). Effects of anthropogenic emissions on aerosol formation from isoprene and monoterpenes in the southeastern United States. *Proceedings of the National Academy of Sciences of the United States of America*, *112*(1), 37–42. https://doi.org/10.1073/pnas.1417609112

Xu, Z., Liu, M., Zhang, M., Song, Y., Wang, S., Zhang, L., et al. (2019). High efficiency of livestock ammonia emission controls in alleviating particulate nitrate during a severe winter haze episode in northern China. *Atmospheric Chemistry and Physics*, *19*, 5605–5613. https://doi.org/10.5194/acp-19-5605-2019

Zhang, X., Wu, Y., Liu, X., Reis, S., Jin, J., Dragosits, U., et al. (2017). Ammonia emissions may be substantially underestimated in China. *Environmental Science & Technology*, *51*(21), 12,089–12,096. https://doi.org/10.1021/acs.est.7b02171

Zheng, B., Tong, D., Li, M., Liu, F., Hong, C., Geng, G., et al. (2018). Trends in China's anthropogenic emissions since 2010 as the consequence of clean air actions. *Atmospheric Chemistry and Physics*, *18*(19), 14,095–14,111. https://doi.org/10.5194/acp-18-14095-2018

Zhou, M., Zhang, Y., Han, Y., Wu, J., Du, X., Xu, H., et al. (2018). Spatial and temporal characteristics of $PM_{2.5}$ acidity during autumn in marine and coastal area of Bohai Sea, China, based on two-site contrast. *Atmospheric Research*, *202*, 196–204. https://doi.org/10.1016/j.atmosres.2017.11.014